Lévy Defects in Matrix-Immobilized J aggregates: Tracing Intra-and Inter-Segmental Exciton Relaxation

Larry Lüer,[a] Sai Kiran Rajendran,[b,c] Tatjana Stoll,[b] Lucia Ganzer,[b] Julien Rehault,[b,d] David M. Coles,[e] David Lidzey, [e] Tersilla Virgili,[b] and Giulio Cerullo.[b]*

a) IMDEA Nanociencia, C/Faraday 9, 28049 Cantoblanco (Madrid), Spain,

b) IFN-CNR, Dipartimento di Fisica, Politecnico di Milano, Piazza L. da Vinci 32, 20133 Milano, Italy

c) School of Physics and Astronomy, University of St. Andrews, St. Andrews, Fife, KY16 9SS (UK)

d) Paul Scherrer Institut, 5232 Villigen PSI, Switzerland

e) University of Sheffield, Department of Physics and Astronomy, Sheffield S3 7RH (UK)

Corresponding Author

* larry.luer@imdea.org, Tel.: 0034 91 2998782

Abstract

One-dimensional J aggregates present narrow and intense absorption and emission spectra which are interesting for photonics applications. Matrix immobilization of the aggregates, as required for most device architectures, has recently been shown to induce a non-Gaussian (Lévy type) defect distribution with heavy tails, expected to influence exciton relaxation. Here we perform two-dimensional electronic spectroscopy (2DES) in one-dimensional J aggregates of the cyanine dye TDBC, immobilized in a gel matrix, and we quantitatively model 2DES maps by non-linear optimization coupled to quantum mechanical calculations of the transient excitonic response. We find that immobilization causes strongly non-Gaussian off-diagonal disorder, leading to a segmentation of the chains. Inter-segmental exciton transfer is found to proceed on the picosecond time scale, causing a long-lasting excitation memory. These findings can be used to inform the design of optoelectronic devices based on J aggregates, as they allow for control of exciton properties by disorder management.

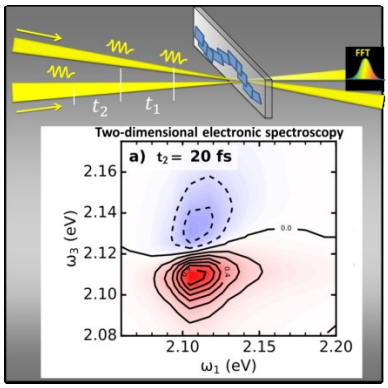

J aggregates are arrangements of conjugated molecules whose lowest energetic optical transitions from the electronic ground state are excitonically coupled such that intense and red-shifted absorption and emission bands arise, and the coupling to intramolecular vibronic modes

is reduced. [1, 2, 3, 4, 5, 6] These properties of J aggregates open up a broad range of applications to biosensors,[7] photoreceptors,[8] dye-sensitized solar cells[9] and, combined with optical cavities[10] and quantum dots, to the study of light harvesting and energy transfer (ET).[11] Owing to the low dimensionality, disorder effects have a profound influence on the optical as well as transport properties of excitons in J aggregates. Disorder leads to fluctuations in the monomer transition energies (diagonal disorder) as well as in the coupling to the neighboring monomers (off-diagonal disorder). [12,13,14,15,16] In homogenous media, a normal distribution of the respective matrix elements ("Gaussian disorder") is often a good approximation to describe J aggregates.[17]

Optoelectronic devices typically require the J aggregates to be immobilized on a surface or in an inert matrix. This immobilization adds a finite number of very specific electrostatic interactions causing non-Gaussian static disorder. It has been predicted that so-called "heavy-tailed Lévy distributions" can have a drastic effect on the exciton properties of J aggregates,[18, 19, 20] Recently, the existence of non-Gaussian distributions has been demonstrated in isolated 1D chains of perylene bisimide (PBI) by the observation of a red-shifted emission in single molecule spectroscopy.[21] In contrast, Sorokin and co-workers ascribed red emission in Pseudo - IsoCyanine (PIC) aggregates in a layer-by-layer grown film to exciton self-localization, rejecting a contribution from non-Gaussian disorder.[22] Understanding the nature of disorder in J aggregates is important not only from a fundamental viewpoint but also for applications for, e.g., "defect management" for the optimization of optoelectronic devices, as recently suggested in ref.[21] .

An unambiguous assessment of the action of non-Gaussian static disorder on exciton dynamics can only be obtained in the time domain. Two-dimensional electronic spectroscopy (2DES) is

ideally suited for this task, since it allows measuring the full third-order nonlinear optical response of the system under study, providing simultaneously high temporal and spectral resolution. [23, 24] PIC J aggregates in homogeneous medium have been studied by 2DES and qualitatively modeled by a Frenkel Hamiltonian and modified Redfield theory. [25] However, to understand and possibly control the effect of non-Gaussian static disorder on exciton dynamics, a quantitative modeling of 2DES maps from immobilized J aggregates is necessary but has not been performed so far.

Quantitative modeling of transient absorption data by global fitting[26] is successful whenever the interplay of a few well-distinguished excited states is studied. [27,28] This approach is not directly applicable to J aggregates, where exciton relaxation must be described in a continuum of states whose spectral properties can only be obtained by appropriate quantum mechanical models, causing a severe penalty in computational effort.[25,29,30] Including such a calculation into an iterative non-linear optimization scheme is thus prohibitive, especially when ballistic (coherent) and stochastic (incoherent, diffusive) exciton transport need to be distinguished.[31] Moreover, recently the validity of modified Redfield theory for molecular aggregates was challenged.[32,33]

Here we perform 2DES on one-dimensional J aggregates of the cyanine dye TDBC immobilized in a gel matrix and demonstrate a novel procedure for the quantitative modeling of the 2DES maps by non-linear optimization. We first use quantum mechanical models to calculate the excited state spectra of the continuum of exciton states. In a second step, we use these spectra as basis states in a global fitting scheme. The decisive reduction in calculation time is thus achieved by taking exciton dynamics out of the quantum mechanical calculations. We find that non-Gaussian static off-diagonal disorder is able to reproduce both linear absorption spectra and

2DES maps; the concomitant segmentation of the 1D chain is confirmed by the observation of slow, diffusive inter-segmental exciton transport.

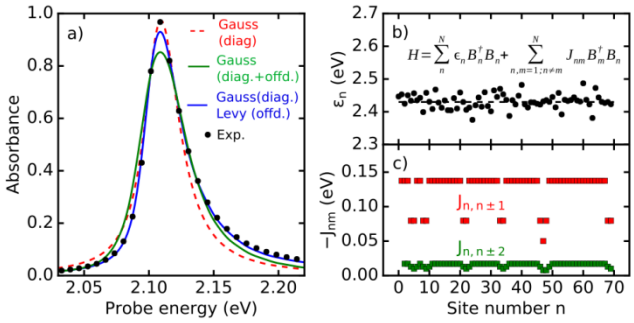

Figure 1. (a) Ground state absorption spectrum (black symbols), best fit assuming only Gaussian diagonal disorder (red dashed line), both diagonal and off-diagonal Gaussian disorder (green line) and best fit assuming Gaussian diagonal disorder and heavy tailed Levy type off-diagonal disorder (blue line). b) and c) Diagonal and off-diagonal matrix elements, respectively, of the Frenkel exciton Hamiltonian whose expression is given in panel b) for a typical disorder realization for the blue curve in panel a). In panel c), only the nearest – and next-nearest neighbor couplings are given (red and green squares, respectively).

Figure 1a shows the ground state absorption (GSA) spectrum of TDBC aggregates in gel matrix, displaying a strongly asymmetric isolated band peaking at 2.11 eV. In TDBC J aggregates in water this band has been qualitatively modeled by a Frenkel exciton model, assuming uncorrelated Gaussian diagonal disorder.[17] Our immobilized J aggregates show a significantly stronger asymmetry in the GSA spectrum than those of ref.[17]; Since immobilization is not expected to act on the vibronic coupling of the J aggregate band, we conjecture that this additional asymmetry derives from an additional contribution to exciton localization caused by immobilization of the one-dimensional chain. It is known that exciton localization causes an

energetic offset between the most strongly allowed fundamental exciton transition and higher energetic ones, which contribute up to 10% of the total oscillator strength of the J aggregate. If exciton localization is caused by Gaussian disorder, then the maximum achievable asymmetry is limited by inhomogeneous broadening of the resulting ensemble spectra (see Supporting Information).

Disorder model	**Lorentzian width Λ (meV)**	**Gaussian width (meV)**	**Error squared**	**Number of defects**
Diag.: Gauss Off-diag.: None	12.8(7)	20(2)	0.66	0
Diag.: Gauss; Off-diag.: Gauss	6.8(3)	29.5(2)	0.43	0
Diag.: Gauss Off-diag.: Lévy	**7.74(4)**	**22.46(7)**	**0.02**	7

Table 1. Fit parameters for the fits in Fig. 1a: width of the Lorentzian lineshape for each exciton state, width of the Gaussian distribution of ε_n , see Fig. 1b. Additionally, the squared error is given for the best fit and the number of traps causing a Lévy type distribution. Values in brackets are standard deviations of the last digit.

We achieved a nearly perfect fit of the GSA spectrum (solid blue line in Fig. 1a) by assuming topological defects, statistically distributed along the aggregate chain, that reduce the inter-site coupling and thus introduce off-diagonal disorder in addition to Gaussian diagonal disorder. Table 1 summarizes the best fit parameters and the corresponding squared error, showing that Lévy-type off-diagonal disorder yields a squared error that is more than one order of magnitude lower than any other disorder model that we applied. The distribution of site energies ε_n and coupling parameters J_{nm} is shown in Fig. 1 b and c, respectively, for a typical realization of the resulting Hamiltonian. As shown in Fig. 1c, off-diagonal disorder is non-Gaussian and heavy tailed (Lévy type) in the sense that we have a small number of defects with very low coupling strength besides a large number of identical "ideal" coupling strengths. We validated this result by excluding the influence of edge effects of the finite aggregate size and by including non-Gaussian diagonal disorder in the calculations (see Supporting Information, Fig. S2). This allows us to describe disorder in immobilized TDBC aggregates as Gaussian on the diagonal, caused e.g. by slow thermally allowed torsional modes, while the strongly non-Gaussian distribution of off-diagonal values points to very specific, localized defects, caused by interactions between TDBC and the host, or by a folding of the chains.

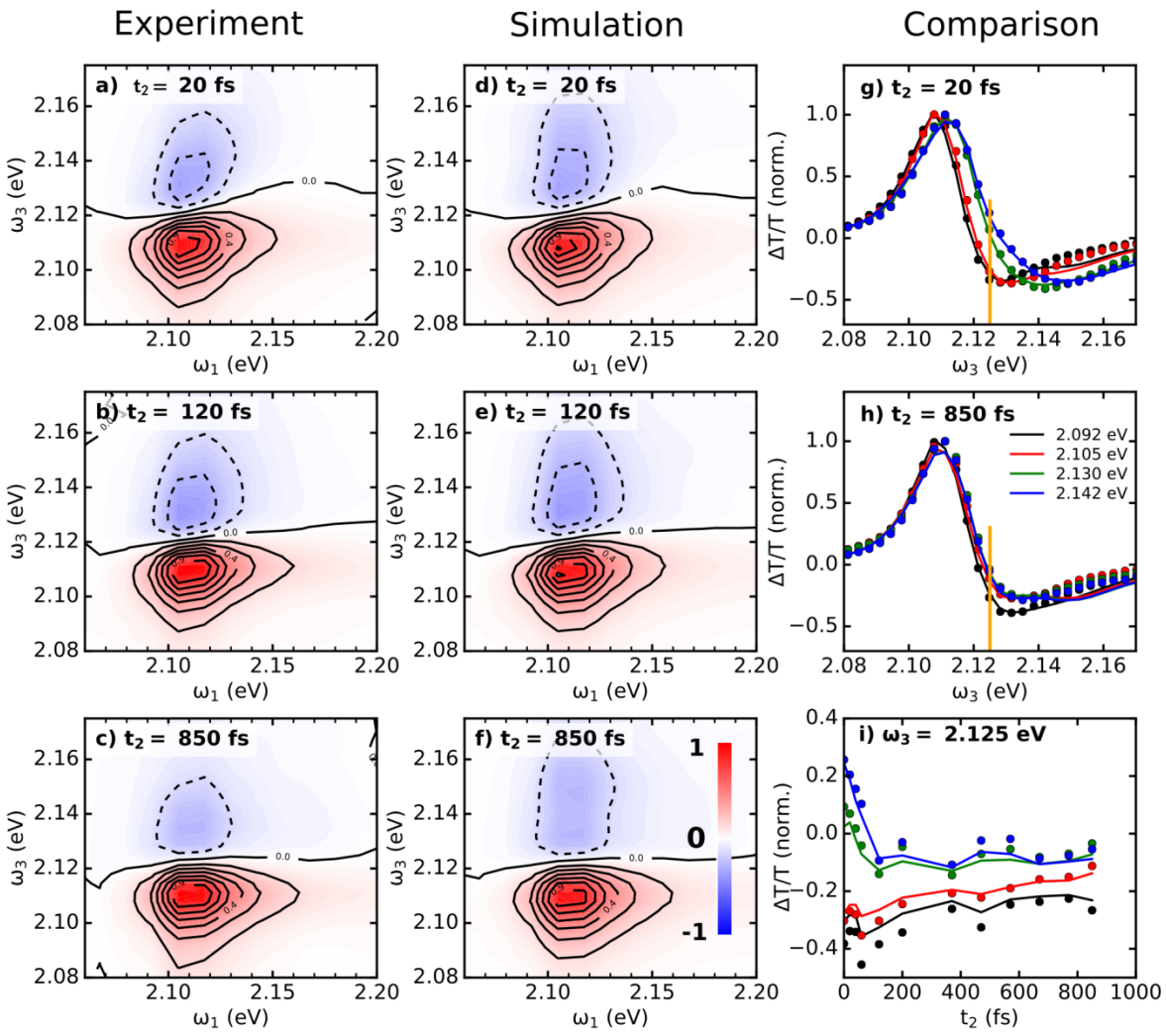

Figure 2.Normalized experimental 2DES maps at waiting times of t_2 = 20, 120 and 850 fs (panel a b, and c, respectively) and corresponding simulations (panel d, e and f, respectively). In panels g and h, vertical intersections through panels a and c, respectively, are given as symbols, while vertical intersections through panels d and f, respectively, are given as lines. Excitation energies ω_1 are color coded as given in panel h. Orange vertical lines indicate the detection energy used to trace the excitation memory in the time domain. Panel i: Normalized 2DES signal at ω_3 = 2.125 eV for excitation energies ω_1 color coded as in panel h.

Figure 2 a, b, c shows a typical set of 2DES maps for waiting times t_2 = 20, 120, and 850 fs, respectively, as a function of excitation frequency ω_1 and detection frequency ω_3. The 2DES maps display the typical features of J aggregates,[25,17] namely a strong positive differential transmission ($\Delta T/T$) peak composed of contributions from photobleaching (PB) and stimulated emission (SE) close to the peak of the linear absorption spectrum (compare with Fig. 1A), and a negative photoinduced absorption (PA) peak, slightly blue-shifted in the detection energy, which is due to transitions from the one- to the two-exciton band. At early times (Fig. 2a), the zero crossing line between PB/SE and PA is strongly diagonally elongated, showing that dephasing and exciton relaxation have not been completed yet.[17, 25] Even after 850 fs, the zero crossing line is still not fully horizontal, which means that there is still significant excitation memory. To emphasize this observation, we show in Fig. 2g, h $\Delta T/T$ spectra (symbols), obtained as vertical intersections through the 2DES maps in Fig. 2a and c, respectively, and normalized to the PB maximum. At t_2 = 20 fs (Fig. 2g), both depth and position of the PA band depend strongly on the excitation energy. For higher excitation energies, the PA band is shifted towards higher detection energies, which is caused by a larger relative contribution of higher energy exciton states, a clear sign of an excitation memory, that is, an exciton distribution that depends on the excitation energy ω_1 even for $t_2 > 0$. It is important to note that this excitation memory, albeit weaker, is still present at waiting times as long as 850 fs, see Fig. 2h. This means that in immobilized TDBC aggregates thermal equilibrium of the exciton population in the available density of states is only reached on the picosecond timescale.

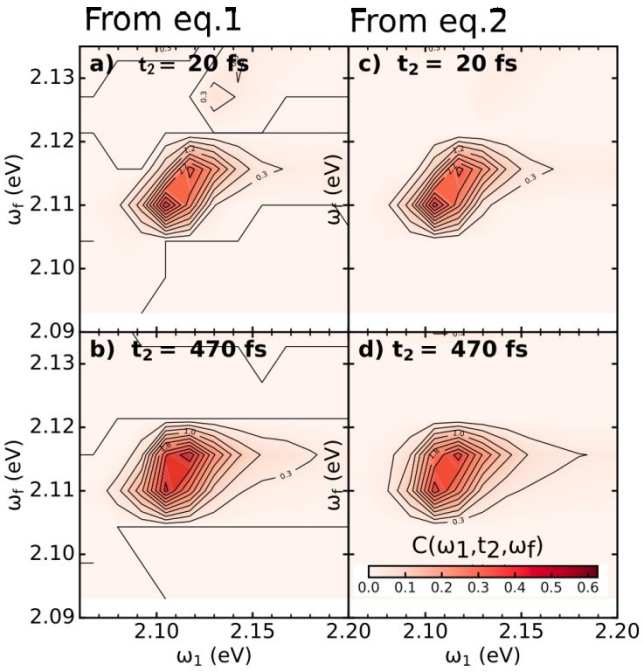

Figure 3. Exciton density $C(\omega_1, \omega_f, t_2)$ (in arbitrary units) for two different waiting times t_2 (panels a, b), resulting from the global fits in fig.2, and numerical reproduction according to a dispersive rate equation model (Eq. 3, panels d and e). A scale bar is given in panel d) for the exciton density in arbitrary units, valid for panels a, b, c, and d.

In order to visualize the dynamics of the loss of excitation memory, we plot the values of the normalized ΔT/T spectra at ω_3 = 2.125 eV, slightly above the peak of the GSA spectrum (see orange vertical lines in Fig. 2g, h) as a function of waiting time t_2. For excitation energies below the GSA maximum, this value increases over time, a clear sign of uphill ET leading to a greater relative occupation of higher energetic excitons. For excitation energies higher than the GSA maximum, the value decreases over time, which is caused by energetically downhill ET. It is important to observe that detailed balance is not attained within our measured range of t_2 times. Detailed balance would in fact lead to a convergence of the ΔT/T values for all excitation

energies after long waiting times and thus to a loss of excitation memory, which is not achieved within our temporal observation window.

We quantitatively model the 2DES maps by a global fitting scheme, minimizing the squared error between the experimental 2DES map and the simulated one which is calculated by

$$\frac{\Delta T}{T}(\omega_1, t_2, \omega_3) \approx -\Delta A(\omega_1, t_2, \omega_3) = -d_s \cdot C\left(\omega_1, t_2, \overline{\omega_f}\right) \cdot \sigma\left(\omega_3, \overline{\omega_f}\right). \quad (1)$$

Herein, d_s is the film thickness, $C\left(\omega_1, t_2, \overline{\omega_f}\right)$ is the concentration of excitons in an eigen energy range with average $\overline{\omega_f}$ at waiting time t_2 after excitation of the aggregate with energy ω_1 at time zero, and $\sigma\left(\omega_3, \overline{\omega_f}\right)$ is the matrix of nonlinear transient absorption spectra (along the probe energy axis ω_3) of excitons of average energy $\overline{\omega_f}$ which is known from quantum mechanical simulations. The derivation of Eq. 1 is shown in the supporting information; note that the integral in Eq. S5 is replaced by the summing procedure inherent to matrix multiplication in Eq. 1. Nonlinear optimization of Eq. 1 (for details see supporting information) delivers the time-dependent exciton dynamics $C\left(\omega_1, t_2, \overline{\omega_f}\right)$. The fits of the 2DES maps, shown in Fig. 2 d, e, and f (for the residuals see supporting information) and as lines in Fig. 2 g, h and i, are in very close agreement with the experimental data. The resulting exciton dynamics $C\left(\omega_1, t_2, \overline{\omega_f}\right)$ is shown in Fig.3 a and b. For t_2 = 20 fs (panel a) the maximum exciton density as function of excitation energy is diagonally elongated, showing that the excitons present at that early waiting time are still close to the respective excitation energies. This means that inter-segmental ET is not significantly active on very early time scales. The exciton distribution at t_2 = 770 fs (panel b) is more independent on the excitation energy ω_1, owing to the fact that, on this time scale, significant inter-segmental ET has occurred. However a closer inspection shows that excitation

memory is still significant. Symbols in Fig 4a show the ratio $C\left(\omega_1, t_2, \overline{\omega_f} = 2.117\ eV\right)/$ $C\left(\omega_1, t_2, \overline{\omega_f} = 2.112\ eV\right)$. This ratio depends on the excitation energy ω_1 and on the waiting time; even after long times the ratios are still different, demonstrating the persistence of an excitation memory. Note that downward ET is much faster than upward ET (compare green symbols to red and black ones, respectively).

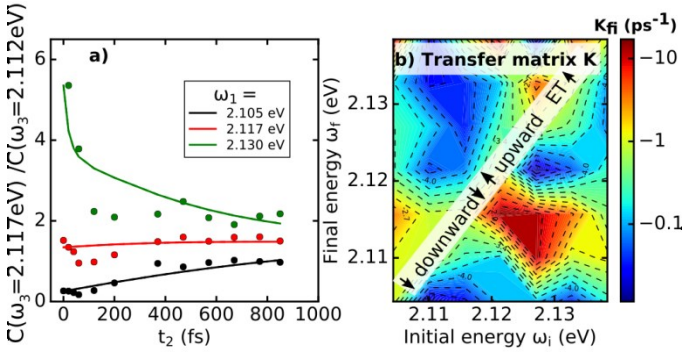

Figure 4. a) Dynamics of excitation memory loss. Different colors refer to different excitation energies, see legend. Symbols: from global fits to Fig.2; lines: from numerical reproductions according to Eq. 2. b): Transfer matrix K on a logarithmic color scale.

Our final goal is to reproduce the dynamics of loss of excitation memory (the symbols in Fig. 3c) by a rate equation model. Using the discretized set of exciton states from Eq.1, the exciton dynamics can be described by a system of ordinary differential equations:

$$\frac{dC(t_2)}{dt} = K \cdot C(t_2) \tag{2}$$

where K is the transfer matrix in which each off-diagonal matrix element $k_{f,i}$ refers to the first order transfer rate constant between the initial exciton state i and the final exciton state f. Diagonal elements $k_{i,i}$ refer to the overall decay of the initial state i and are given by $k_{i,i} = \sum_{f \neq i} -k_{f,i}$. This model does not include relaxation to the ground state which occurs only on a much longer time scale than exciton equilibration. Exciton annihilation, on the other hand, has been shown for TDBC in water to occur even on sub-picosecond time scales.[17] In our measurements on TDBC in gel matrix, we found that exciton annihilation can be neglected for the excitation fluences used in Fig. 2 (for details, see supporting information).

Using Eq. 2 we achieved an excellent reproduction of the exciton distribution for all excitation energies, compare Fig.3 d to a and Fig.3 e to b, respectively. Fits for all waiting times are given in the Supporting Information. Most importantly, we are able to reproduce the dynamics of excitation memory loss without significant deviation, see solid curves in Fig. 4a. Figure 4b shows the transfer matrix K in a false color representation using a logarithmic color scale (see color bar). Due to the multitude of free parameters, we expect substantial uncertainty in the single transfer matrix elements. For this reason, we focus our discussion only on those features which were observed in all transfer matrices that we obtained (see Supporting information part E). We generally observe, in Fig 4b as well as in Fig. S10, that the matrix elements for downward ET (found in the lower triangle) are typically orders of magnitude faster than those for upward ET (found in the upper left triangle This points to a strongly different inter-state coupling involved into both processes. Energetically downhill ET can be caused by on-segment relaxation of a hot exciton state, proceeding in less than 100 fs. On the other hand, energetically upward ET typically cannot proceed on-segment because the spacing of the excitonic levels is too large. Therefore upward ET typically involves inter-segment transfer steps which due to reduced

coupling are much slower; as Figure 4b shows, typical upward ET rate constants are in the range of 1 – 10 ps. These findings are in agreement with our picture of topological defects causing a hard segmentation of the one-dimensional chain, leading to a clear distinction between intra-segment and inter-segmental ET processes This distinction – and the concomitant vastly different exciton transfer constants - has recently been predicted theoretically by a model in which a heavy tailed Lévy distribution has been assumed for the diagonal disorder.[3420]

These findings are relevant for the optimization of optoelectronic devices based on J aggregates. The absence of non-Gaussian contributions to the diagonal disorder, even when the aggregates are immobilized, guarantees the motional narrowing causing the sharp and strongly allowed J aggregate band. The observed strongly non-Gaussian off-diagonal disorder, on the other hand, causes a hard segmentation which presents a handle for device technology optimizing exciton motion. Segmentation preserves exciton position and energy, thus preventing their diffusion towards deactivation centers. However, care must be taken that the segments are not too short, or else the positive effect of motional narrowing of the J aggregate bands would be reduced. In aqueous solutions of TDBC aggregates, an exciton delocalization length of about 14 units has been found resulting from pure Gaussian disorder;[17] therefore the average segment length of about 12 units that we found in Fig.1, seems appropriate to match the advantages of infinite J aggregates (narrow and strong absorption and emission bands) with those of isolated oligomers (high definition of excited states and relaxation pathways). A further possibility to engineer J aggregate properties would be to deliberately cause segmentation into short and long segments, allowing for vectorial (directional) ET towards a reaction site for photovoltaic or sensing applications.

In conclusion, we have used 2DES to study exciton relaxation dynamics in the prototypical J aggregate TDBC immobilized in a gel matrix. We have quantitatively modeled 2DES maps by a nonlinear optimization technique incorporating quantum mechanical calculations. Our best fits produced a phenomenological dephasing parameter of λ = 8 meV (causing a Lorentzian broadening of the linear and nonlinear spectra), a Gaussian diagonal disorder of 22 meV, and an off-diagonal disorder characterized by one defect approximately every 10 monomers, normally distributed along the chain. We find that immobilization causes strongly non-Gaussian (heavy-tailed Lévy type) off-diagonal disorder, while diagonal disorder remains Gaussian as in homogeneous media. Immobilization therefore causes a static segmentation of the one-dimensional chains. The resulting inter-segmental ET causes a long lasting excitation memory which can be exploited for optoelectronic applications.

ACKNOWLEDGMENT

LL thanks the EC for financial support by the cofunded Amarout program and the Spanish Ministry for economy and competitiveness (plan nacional, Project MultiCrom). GC acknowledges financial support by the European Research Council (ERC-2011-AdG No. 291198).

Experimental and Computational Methods:

Sample preparation. TDBC is the sodium salt of 1,18-diethyl-3,38-bis~4-sulfobutyl-5,58,6,68-tetrachloro-benzimidazolo carbocyanine, which forms linear J aggregates in aqueous solution.[17] Immobilized TDBC J aggregates were prepared in a gel matrix at a TDBC concentration of about 4.5% weight. Details are found in ref (35).

Two-dimensional electronic spectroscopy. 2DES was performed in the partially collinear pump-probe geometry[36] using visible pulses generated by a non-collinear optical parametric amplifier (NOPA)[37] pumped by 100-fs, 800-nm pulses at 1 kHz repetition rate from a regeneratively amplified Ti:Sapphire laser (Coherent Libra). The NOPA pulses are compressed to 8-fs duration by multiple bounces on chirped mirrors and used both for excitation and detection. A collinear phase-locked pump pulse pair, delayed by the coherence time t_1, is generated by a passive common-mode birefringent interferometer[38] based on a sequence of α-barium borate wedges and plates. The dispersion introduced by the interferometer is compensated by an additional pair of chirped mirrors placed on the pump beam path. Details on our 2DES setup are reported in ref.(39).

Numerical model. We use the Frenkel exciton Hamiltonian to calculate all available excitons of the one- and two-exciton band of the J aggregate. We first tune our aggregate model by fitting the linear absorption spectrum, varying the parameters modeling disorder. Using the parameters from the best fit of the linear spectrum, we then calculate nonlinear excited state spectra considering only Liouville pathways not involving ET. In a final step, we fit the obtained time-dependent exciton density distribution to a rate equation model to find the transfer matrix. This combination of approaches gives us the unique possibility to trace back the experimentally measured exciton dynamics to the characteristics of the aggregate that are described by the system Hamiltonian. The detailed fitting procedure is given in the Supporting information.

ASSOCIATED CONTENT

Supporting Information is available free of charge in pdf format Contents: (A) Calculation of exciton states in linear J aggregates with heavy tail states, (B) Calculation of linear absorption

and 2DES maps, (C) Comparison of models, (D) Complete results of global fitting, (E) Pump intensity dependence, (F) Details of Experimental Method.

References:

(1) Jelley, E. E. Spectral Absorption and Fluorescence of Dyes in the Molecular State. *Nature* **1936**, *138* (3502), 1009–1010.

(2) Würthner, F.; Kaiser, T. E.; Saha-Möller, C. R. J-Aggregates: From Serendipitous Discovery to Supramolecular Engineering of Functional Dye Materials. *Angew. Chemie Int. Ed.* **2011**, *50* (15), 3376–3410.

(3) Czikkely, V.; Forsterling, H. D.; Kuhn. Light Absorption and Structure of Aggregates of Dye Molecules. H. *Chem. Phys. Lett.* **1970**, *6* (1), 11.

(4) Bücher, H.; Kuhn, H. Scheibe Aggregate Formation of Cyanine Dyes in Monolayers. *Chem. Phys. Lett.* **1970**, *6* (3), 183–185.

(5) Akselrod, G. M.; Tischler, Y. R.; Young, E. R.; Nocera, D. G.; Bulovic, V. Exciton-Exciton Annihilation in Organic Polariton Microcavities. *Phys. Rev. B* **2010**, *82* (11), 113106.

(6) Marciniak, H.; Li, X.-Q.; Würthner, F.; Lochbrunner, S. One-Dimensional Exciton Diffusion in Perylene Bisimide Aggregates. *J. Phys. Chem. A* **2011** 115(5), 648-654.

(7) Mati, S.S.; Chall, S.; Bhattacharya, S.C. Aggregation-Induced Fabrication of Fluorescent Organic Nanorings: Selective Biosensing of Cysteine and Application to Molecular Logic Gate. *Langmuir* **2015**, 31(18), 5025-5032.

(8) Law, K. Y. Organic Photoconductive Materials: Recent Trends and Developments. *Chem. Rev.* **1993**, 93, 449 – 486.

(9) Sayama, K.; Tsukagoshi, S.; Hara, K.; Ohga, Y.; Shinpou, A.; Abe, Y.; Suga, S; Arakawa, H. Photoelectrochemical Properties of J Aggregates of Benzothiazole Merocyanine Dyes on a Nanostructured TiO2 Film. *J. Phys. Chem.* B **2002**, 106, 1363-1371.

(10) Lidzey, D.; Bradley, D.; Virgili, T.; Armitage, A.; Skolnick, M.; Walker, S. Room Temperature Polariton Emission from Strongly Coupled Organic Semiconductor Microcavities. *Phys. Rev. Lett.* 1999, 82, 3316-3319.

(11) Walker, B. J.; Bulovic, V.; Bawendi, M. G. Quantum Dot/J-Aggregate Blended Films for Light Harvesting and Energy Transfer. *Nano Lett.* **2010**, 10(10), 3995 -3999.

(12) Han, J.; Zhang, H.; Abramavicius, D. Exchange Narrowing and Exciton Delocalization in Disordered J Aggregates: Simulated Peak Shapes in the Two Dimensional Spectra. *J. Chem. Phys.* **2013,** 139, 034313.

(13) Butkus, V.; Gelzinis, A.; Valkunas, L. Quantum Coherence and Disorder-Specific Effects in Simulations of 2D Optical Spectra of One-Dimensional J-aggregates. *J. Phys. Chem. A* **2011**, 115(16), 3876–3885.

(14) Ke, Z.; Liu, Z.; Zhao, Z. Visualization of Hot Exciton Energy Relaxation from Coherent to Diffusive Regimes in Conjugated Polymers: A Theoretical Analysis. *J.Phys.Chem.Lett.* **2015**, 6(9), 1741−1747.

(15) Butkus, V.; Zigmantas, D.; Abramavicius, D.; Valkunas, L. Distinctive Character of Electronic and Vibrational Coherences in Disordered Molecular Aggregates. *Chem. Phys. Lett.* **2013**, 587, 93–98

(16) Ohta, K.; Yang, M; Fleming, G. R. Ultrafast Exciton Dynamics of J-aggregates in Room Temperature Solution Studied by Third-Order Nonlinear Optical Spectroscopy and Numerical Simulation Based on Exciton Theory. *J. Chem. Phys.* **2001**, 115(16), 7609-7621.

(17) Van Burgel, M.; Wiersma, D. A.; Duppen, K. The Dynamics of One-Dimensional Excitons in Liquids. *J. Chem. Phys*. **1995**, 102(1), 20.

(18) Levy, P. Théorie des Erreurs: la Loi de Gauss et les Lois Exceptionelles [Theory of Errors: The Law of Gauss and the Exceptional Laws]. 1924, *Bull. Soc. Math. Fr.* **1924**, 52, 49-85.

(19) Eisfeld, A.; Vlaming, S. M.; Malyshev, V. A.; Knoester. Excitons in Molecular Aggregates with Lévy-Type Disorder: Anomalous Localization and Exchange Broadening of Optical Spectra. *Phys. Rev. Lett.* **2010**, 105, 137402.

(20) Lim, J., Palaček, D., Caycedo-Soler, F., Lincoln, C. N., Prior, J., von Berlepsch. H., Huelga, S. F., Plenio, M. B., Zigmantas, D., Hauer, J. Vibronic Origin of Long-Lived Coherence in an Artificial Molecular Light Harvester. *Nat. Comm.* 2015, 6:7755

(21) Merdasa, A.; Jiménez, A. J.; Camacho, R.; Meyer, M.; Würthner, F.; Scheblykin, I. G. Single Lévy States–Disorder Induced Energy Funnels in Molecular Aggregates. *Nano Lett.* **2014**, 14(12), 6774−6781.

(22) Sorokin, A. V.; Pereverzev, N. V.; Grankina, I. I.; Yefimova, S. L.; Malyukin, Y. V. Evidence of Exciton Self-Trapping in Pseudoisocyanine J-Aggregates Formed in Layered Polymer Films. *J. Phys. Chem. C* **2015**, 119(49), 27865−27873.

(23) Hochstrasser, R. M. Two-Dimensional Spectroscopy at Infrared and Optical Frequencies. *Proc. Natl. Acad. Sci. U.S.A.* **2007**, 104(36), 14190-14196.

(24) Mukamel, S. Multidimensional Femtosecond Correlation Spectroscopies of Electronic and Vibrational Excitations. *Annu. Rev. Phys. Chem*. **2000**, 51, 691-729.

(25) Stiopkin, I.; Brixner, T.; Yang, M.; Fleming, G. R. Heterogeneous Exciton Dynamics Revealed by Two-Dimensional Optical Spectroscopy. *J. Phys. Chem. B* **2006**, 110(40), 20032-20037

(26) van Stokkum, I. H. M.; Larsen, D. S.; van Grondelle, R. Global and Target Analysis of Time-Resolved Spectra. *Biochim. Biophys. Acta – Bioenerg*. **2004**, 1657 (2-3) 82–104.

(27) Consani, C.; Koch, F.; Panzer, F.; Unger, T.; Köhler, A.; Brixner, T. Relaxation Dynamics and Exciton Energy Transfer in the Low-Temperature Phase of MEH-PPV. *J. Chem. Phys.* **2015**, 142, 212429.

(28) Lüer, L.; Carey, A.-M.; Henry, S.; Maiuri, M.; Hacking, K.; Polli, D.; Cerullo, G.; Cogdell, R. J. Elementary Energy Transfer Pathways in Allochromatium Vinosum Photosynthetic Membranes. *Biophys. J.* **2015**, 109(9) 1885–1898.

(29) Dijkstra, A. G.; Jansen, T.L.C.; Knoester, J. Localization and Coherent Dynamics of Excitons in the Two-Dimensional Optical Spectrum of Molecular J-Aggregates. *J. Chem. Phys*. **2008**, 128(16), 164511.

(30) Agarwal, R.; Rizvi, A. H.; Prall, B. S.; Olsen, J. D.; Hunter, C. N.; Fleming, G. R. ature of Disorder and Inter-Complex Energy Transfer in LH2 at Room Temperature: A Three Pulse Photon Echo Peak Shift Study. *J. Phys. Chem. A* **2002**, 106(33), 7573-7578.

(31) Valleau, S.; Saikin, S. K.; Yung, M.-H.; Aspuru-Guzik, A. Exciton Transport in Thin-Film Cyanine Dye J-Aggregates. *J. Chem. Phys*. **2012**, 137, 034109.

(32) Kreisbeck, C.; Aspuru-Guzik, A. Efficiency of energy funneling in the photosystem II supercomplex of higher plants. *Chem. Sci.* **2016**, 7, 4174-4183.

(33) Gelzinis, A.; Abramavicius, D.; Valkunas, L. Absorption Lineshapes of Molecular Aggregates Revisited. *J. Chem. Phys*. **2015** 142, 154107.

(34) Vlaming, S.M., Malyshev, V.A., Eisfeld, A., Knoester, J. Subdiffusive Exciton Motion in Systems with Heavy-Tailed Disorder. *J. Chem. Phys.* 2013, 138, 214316

(35) Rajendran, S. K.; Wang, W.; Brida, D.; De Sio, A.; Sommer, E.; Vogelgesang, R.; Coles, D.; Lidzey, D.G.; Cerullo, G.; Lienau, C.; Virgili, T. Direct Evidence of Rabi Oscillations and Antiresonance in a Strongly Coupled Organic Microcavity. *Phys. Rev. B* **2015**, 91(20), 201305.

(36) DeFlores, L. P.; Nicodemus, R. A.; Tokmakoff, A. Two-Dimensional Fourier Transform Spectroscopy in the Pump–Probe Geometry. *Opt. Lett.* **2007**, **32**(20), 2966-2968.

(37) Zavelani-Rossi, M.; Cerullo, G.; De Silvestri, S.; Gallmann, L.; Matuschek, N.; Steinmeyer, G.; Keller, U.; Angelow, G.; Scheuer, V.; Tschudi, T. Pulse Compression Over a 170-THz Bandwidth in the Visible by Use of Only Chirped Mirrors. *Opt. Lett.* **2001**, 26(15), 1155-1157.

(38) Brida, D.; Manzoni, C.; Cerullo, G. Phase-Locked Pulses for Two-Dimensional Spectroscopy by a Birefringent Delay Line. *Opt. Express* **2012**, **37**(15), 3027-3029.

(39) Réhault, J.; Maiuri, M.; Oriana, A.; Cerullo, G. Two-Dimensional Electronic Spectroscopy With Birefringent Wedges. *Rev. Sci. Instrum*. **2014**, 85, 123107.